ELSEVIER

Catalysis Today 79–80 (2003) 219–227

CATALYSIS TODAY

www.elsevier.com/locate/cattod

# Scale up studies on partitioned bubble column reactors with the aid of CFD simulations

J.M. van Baten, R. Krishna*

*Department of Chemical Engineering, University of Amsterdam, Nieuwe Achtergracht 166, 1018 WV Amsterdam, The Netherlands*

**Abstract**

In an earlier publication on partitioned bubble columns [Catal. Today 69 (2001) 165–170], liquid phase residence time distribution was measured in columns of 0.10, 0.15 and 0.38 m diameter at superficial gas velocities, $U_G$, in the range 0.05–0.4 m/s. In the present study, CFD simulations, using two-dimensional Cartesian geometry and the Eulerian framework, are used to provide a theoretical background to our earlier experimental work. Both CFD simulations and experiments show that the (superficial) liquid exchange velocity, $U_{ex}$, at the partition plate is independent of column diameter; the exchange velocity $U_{ex}$ is however found to be a strong function of the open area of the partition plates. The height of the gas cap forming underneath partition plates decreases significantly with increasing column diameter; this is a desirable result from the point of view of scale up.

It is concluded that CFD simulations can be a powerful scale up tool.


*Keywords:* Bubble columns; Churn-turbulent flow regime; Partition; Backmixing; Liquid interchange; Computational fluid dynamics; Gas cap height

## 1. Introduction

Bubble columns are widely used for carrying out gas–liquid reactions in a variety of practical applications in industry [1,2]. They are simple in construction and particularly suited for carrying out relatively slow chemical reactions requiring large liquid hold-ups in the reactor. The scale up of bubble columns is made particularly difficult, because the column hydrodynamics are a strong function of the column diameter, $D_T$. As a consequence, the liquid phase in commercial scale bubble column reactors can be considered practically well-mixed.

In many practical applications, it is desirable to have the liquid phase retain its plug flow character in the commercial reactor. Staging of the liquid phase can be achieved by introducing partition plates; see Fig. 1. Below each partition plate, a gas layer, or gas cap, builds up because of pressure drop considerations. A large gas cap is undesirable, because it represents a waste of reactor space. By adjusting the open (free) area of the partition plates, the exchange of liquid between the compartments can be regulated. The smaller the free area, the lower is the exchange velocity of the liquid phase, $U_{ex}$, leading to a greater suppression of the overall backmixing in the column.

Of the several publications on the influence of partition plates on the hydrodynamics of bubble columns [3–18], only the work of Dreher and Krishna [3] has focused on the influence of column diameter. Dreher and Krishna [3] performed experiments in three

* Corresponding author. Tel.: +31-20-525-7007; fax: +31-20-525-5604.
*E-mail address:* krishna@science.uva.nl (R. Krishna).

0920-5861/03/$ – see front matter © 2003 Elsevier Science B.V. All rights reserved.
doi:10.1016/S0920-5861(03)00008-7

**Nomenclature**

| | |
|---|---|
| AF | acceleration factor, see Eq. (6), dimensionless |
| $C_D$ | drag coefficient, dimensionless |
| $d$ | diameter (m) |
| $D_T$ | column (tower) diameter (m) |
| $D_{ax,L}$ | liquid phase axial dispersion coefficient ($m^2/s$) |
| Eö | Eötvös number, $g(\rho_L - \rho_G)d_b^2/\sigma$ dimensionless |
| $g$ | gravitational constant ($m/s^2$) |
| $\boldsymbol{g}$ | gravity vector ($m/s^2$) |
| $\boldsymbol{M}$ | momentum exchange term ($N/m^3$) |
| $p$ | pressure (Pa) |
| SF | scale factor, see Eq. (6), dimensionless |
| $t$ | time (s) |
| $\boldsymbol{u}$ | velocity vector (m/s) |
| $U_{circ}$ | superficial liquid circulation velocity in empty column or within section of column (m/s) |
| $U_{ex}$ | superficial liquid exchange velocity through partition plate (m/s) |
| $U_G$ | superficial gas velocity (m/s) |
| $U_{trans}$ | superficial transition velocity (m/s) |
| $V_b$ | rise velocity of bubbles (m/s) |

*Greek symbols*

| | |
|---|---|
| $\varepsilon$ | hold-up, dimensionless |
| $\mu$ | viscosity (Pa s) |
| $\sigma$ | surface tension (N/m) |
| $\rho$ | density ($kg/m^3$) |

*Subscripts*

| | |
|---|---|
| ax | axial |
| b | referring to either (small or large) bubble phase |
| G | referring to gas phase |
| k | referring to phase k |
| l | referring to phase l |
| large | referring to large bubble population |
| L | referring to liquid phase |
| small | referring to small bubble population |
| trans | referring to regime transition from homogeneous to heterogeneous |

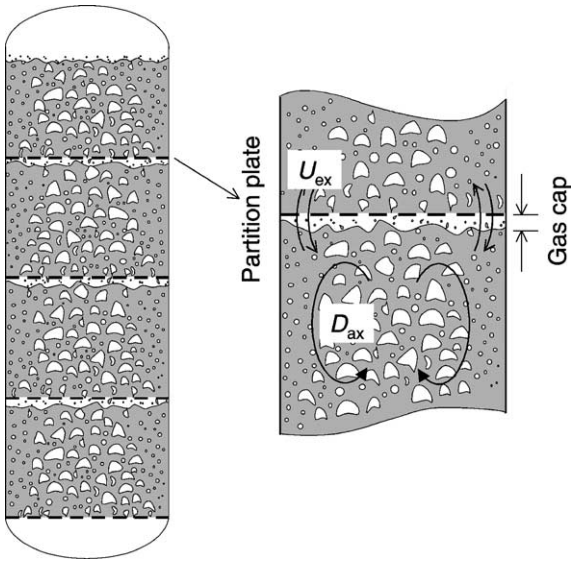


Fig. 1. Schematic diagram of the hydrodynamics of compartmented bubble columns. The inset shows the liquid exchange between compartments, with velocity $U_{ex}$, and the axial dispersion within each compartment.

bubble columns with inner diameters of 0.10, 0.15 and 0.38 m (details of the experimental set-up are available at our web site: http://ct-cr4.chem.uva.nl/partition/). The columns were operated with demineralised water as the liquid phase (batch operation), and air as the gas phase. Perforated plate spargers (holes of 0.5 mm diameter) were used in all columns to distribute the air. The bubble columns were compartmented using perforated brass partition plates, of 1 mm thickness, and having holes of 10 mm diameter. The free, or open, area of the partition plates was 18.6%. In the 0.15 m column, experiments were also carried out with a partition plate have 30.7% open area. Residence time distributions (RTD) of the liquid phase were measured using salt tracer injection and the results were interpreted in terms of a two-parameter model with an axial dispersion model (parameter $D_{ax,L}$) within each compartment, along with liquid interchange (with superficial velocity $U_{ex}$) at the partition plate; see Fig. 1. The values of $D_{ax,L}$ increase strongly with the column diameter; see Fig. 2(a). On the other hand the $U_{ex}$, for a given partition plate (with 18.6% open area) is independent of column diameter; see Fig. 2(b). Increasing the open area of

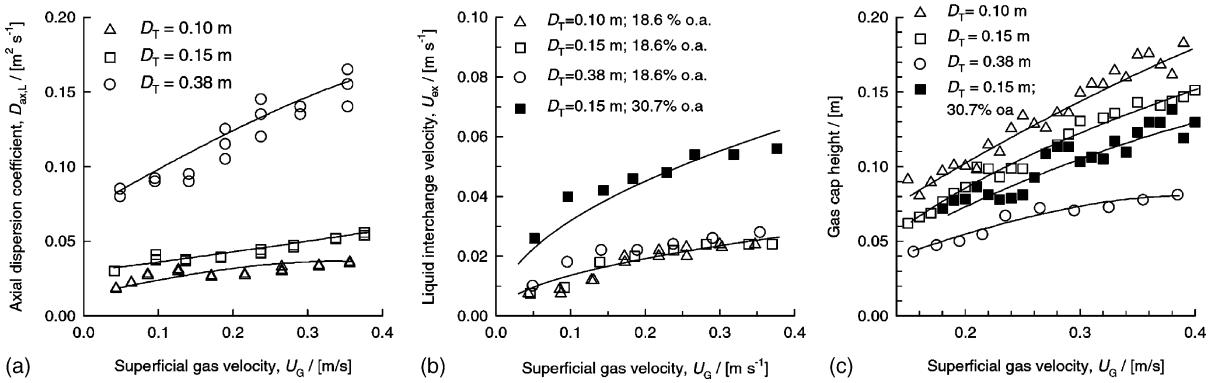


Fig. 2. Experimentally determined parameters for multi-stage bubble column [3]: (a) axial dispersion in empty bubble columns; (b) liquid interchange velocity between compartments; (c) gas cap height below partition plate.

the partition to 30.7% increases $U_{ex}$ significantly; see Fig. 2(b). The gas cap height decreases significantly with increasing column diameter; see Fig. 2(c). This is advantageous from a scale up point of view because a large gas cap height implies unused reaction space. Increasing the open area decreases the gas cap height, but at the cost of increased liquid interchange between compartments.

The primary objective of the present communication is to provide theoretical support to the experimental work of Dreher and Krishna [3] by use of computational fluid dynamics (CFD). CFD techniques have been successfully applied to study scale effects in "empty" bubble columns [19–30]. We extend our earlier CFD approach [23–29] to partitioned bubble columns, and concentrate our attention on the churn-turbulent flow regime that prevails at superficial gas velocities above say 0.05 m/s.

## 2. Eulerian simulations

In the churn-turbulent regime of operation, the bubble sizes vary over a wide range between 1 and 50 mm depending on the operating conditions and phase properties. Our approach for modelling purposes is to assume that in the churn-turbulent flow regime, we have two distinct bubble classes: "small" and "large"; see Fig. 3. The small bubbles are in the size range of 1–6 mm and are either spherical or ellipsoidal in shape depending the physical properties of the liquid. The large bubbles are typically in the range of 20–80 mm range and fall into the spherical cap regime. These bubbles undergo frequent coalescence and break-up.

From the Reilly et al. [32] correlation, it was determined that the superficial gas velocity at the regime transition point for air–water $U_{trans} = 0.034$ m/s. Following the model of Krishna and Ellenberger [31], we assume that in the churn-turbulent flow regime, the superficial gas velocity through the small bubble phase is $U_{trans} = 0.034$ m/s (see Fig. 3). The remainder of the gas ($U_G - U_{trans}$) was taken to rise up the

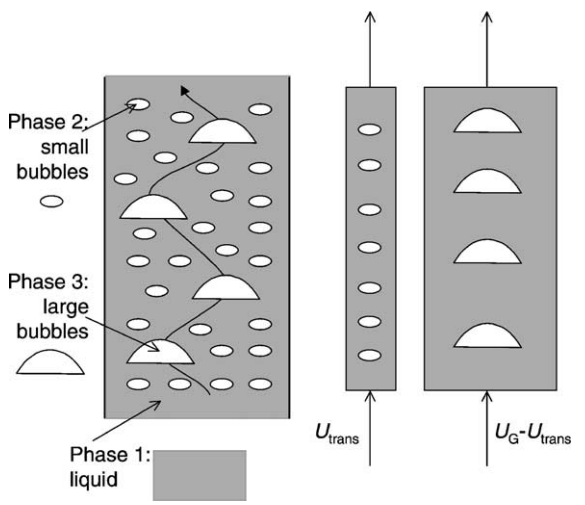


Fig. 3. Schematic of three-phase model used in the Eulerian simulations.

column in the form of large bubbles. This implies that at the distributor, the "large" bubbles constitute a fraction $(U_G - U_{trans})/U_G$ of the total incoming volumetric flow, whereas the "small" bubble constitute a fraction ($U_{trans}/U_G$) of the total incoming flow). Strictly speaking, $U_{trans}$ is a model parameter and its choice has a significant increasing effect on the small bubble hold-up.

For each of the three phases shown in Fig. 3, the volume-averaged mass and momentum conservation equations in the Eulerian framework are given by:

$$\frac{\partial(\varepsilon_k \rho_k)}{\partial t} + \nabla(\rho_k \varepsilon_k \mathbf{u}_k) = 0 \quad (1)$$

$$\frac{\partial(\rho_k \varepsilon_k \boldsymbol{u}_k)}{\partial t} + \nabla(\rho_k \varepsilon_k \boldsymbol{u}_k \boldsymbol{u}_k - \mu_k \varepsilon_k (\nabla \boldsymbol{u}_k + (\nabla \boldsymbol{u}_k)^T)) = -\varepsilon_k \nabla p + \boldsymbol{M}_{kl} + \rho_k \boldsymbol{g} \quad (2)$$

where $\rho_k$, $\boldsymbol{u}_k$, $\varepsilon_k$ and $\mu_k$ represent, respectively, the macroscopic density, velocity, volume fraction and viscosity of the kth phase, $p$ the pressure, $\boldsymbol{M}_{kl}$ the interphase momentum exchange between phase k and phase l and $\boldsymbol{g}$ is the gravitational acceleration. The momentum exchange between either bubble phase (subscript b) and liquid phase (subscript L) phases is given by:

$$\boldsymbol{M}_{L,b} = \frac{3}{4}\rho_L \frac{\varepsilon_b}{d_b} C_D (\boldsymbol{u}_b - \boldsymbol{u}_L)|\boldsymbol{u}_b - \boldsymbol{u}_L| \quad (3)$$

The liquid phase exchanges momentum with both the "small" and "large" bubble phases. No interchange between the "small" and "large" bubble phases has been included in the present model and each of the dispersed bubble phases exchanges momentum only with the liquid phase. The interphase drag coefficient is calculated from equation:

$$C_D = \frac{4}{3}\frac{\rho_L - \rho_G}{\rho_L} g d_b \frac{1}{V_b^2} \quad (4)$$

where $V_b$ is the rise velocity of the appropriate bubble population. We have only included the drag force contribution to $\boldsymbol{M}_{L,b}$ in keeping with the works of Sanyal et al. [21] and Sokolichin and Eigenberger [22]. The added mass force has been ignored in the present analysis. The reason for this neglect is that the focus of the simulations and experiments in this work is on the churn-turbulent flow regime. The distinguishing feature of this regime is the existence of large fast-rising bubbles. These large bubbles do not have a closed wake and the concept of added mass is not applicable. The small bubbles on the other hand do have a closed wake. However, in the churn-turbulent flow regime these bubbles suffer strong recirculations, moving downwards near the wall region. Inclusion of the added mass contributions to the small bubbles led to severe convergence difficulties. The added mass contributions were therefore omitted. Lift forces are also ignored in the present analysis because of the uncertainty in assigning values of the lift coefficients to the small and large bubbles. For the large bubbles, for which Eö $> 40$ holds, literature data suggest the use of a negative lift coefficient, whereas for small bubbles for which typically Eö $= 2$, the lift coefficient is positive [19]. For the continuous, liquid, phase, the turbulent contribution to the stress tensor is evaluated by means of k–$\varepsilon$ model, using standard single-phase parameters $C_\mu = 0.09$, $C_{1\varepsilon} = 1.44$, $C_{2\varepsilon} = 1.92$, $\sigma_k = 1$ and $\sigma_\varepsilon = 1.3$. The applicability of the k–$\varepsilon$ model has been considered in detail by Sokolichin and Eigenberger [22]. No turbulence model is used for calculating the velocity fields of the dispersed "small" and "large" bubble phases.

From visual observations of bubble column operations with the air–water system, the small bubbles were observed to be in the 3–6 mm size range. In the simulations, we chose a small bubble diameter of 4 mm. The rise velocity of air bubbles is practically independent of bubble diameter in this size range and the Harmathy [33] equation for the rise velocity:

$$V_{b,small} = 1.53 \left(\frac{\sigma g}{\rho_L}\right)^{0.25} \quad (5)$$

is used in the simulation model. The large bubble rise velocity was modelled using the approach developed by Krishna et al. [34], which introduces an acceleration factor AF into the Collins relation [35] for the rise of a single spherical cap bubble:

$$V_{b,large} = 0.71\sqrt{g d_{b,large}}\,(SF)\,(AF) \quad (6)$$

The expressions developed by Krishna et al. [34] for the large bubble size and acceleration factor for air–water are used in this work for estimation of the drag coefficient for the large bubble phase; see also [23–26].

A commercial CFD package CFX 4.2 of AEA Technology, Harwell, UK, was used to solve the equations of continuity and momentum. This package is a finite volume solver, using body-fitted grids. The grids are non-staggered and all variables are evaluated at the cell centres. An improved version of the Rhie–Chow algorithm [36] is used to calculate the velocity at the cell faces. The pressure-velocity coupling is obtained using the SIMPLEC algorithm [37]. For the convective terms in Eqs. (1) and (2) hybrid differencing was used. A fully implicit backward differencing scheme was used for the time integration.

Our earlier work [27] had shown that for a quantitative description of the liquid phase dispersion in bubble columns, one must use fully 3D transient simulations. Use of the assumption of cylindrical axi-symmetry leads to a severe under-prediction of the liquid phase dispersion. Fully 3D simulations are, however, computationally very expensive and therefore the strategy we have chosen here is to adopt the 2D Cartesian simulation strategy, without imposing the constraint of axi-symmetry in order to capture the chaotic hydrodynamics. The price we have to pay for adopting the 2D Cartesian strategy is that we should not expect a *quantitative* agreement with experiments. So, our restricted objective is to obtain a *qualitative* underpinning of the experimental results shown in Fig. 2.

Simulations were carried using 2D Cartesian geometry for three column diameters: 0.10, 0.15 and 0.38 m. They are operated at four superficial gas velocities $U_G$ of 0.09, 0.16, 0.23 and 0.30 m/s. All columns were 2 m in height. A partition plate was mounted at a height of 1.0 m, with a plate porosity of either 0.186 or 0.307. The grid used uniform cell spacing in the radial direction; see Fig. 4. All columns had 38 cells in the diameter of the column. At the partition plate, three cells on each side of the plate are modelled as impermeable solids, in total 6/38 of the diameter. The porous part of the partition plate in between these solid ends had porosity corrected in such a way that the above-mentioned total plate porosities were met. Cells of 0.01 m were used in the height of the columns, below 0.95 and above 1.05 m. Around the plate, in the region of 0.95–1.05 m, 100 cells of $1 \times 10^{-3}$ m in height were used. The plate had a thickness of 0.01 m and was located in height between 1.00 and 1.01 m. A total of 290 cells were used in the height of the columns.

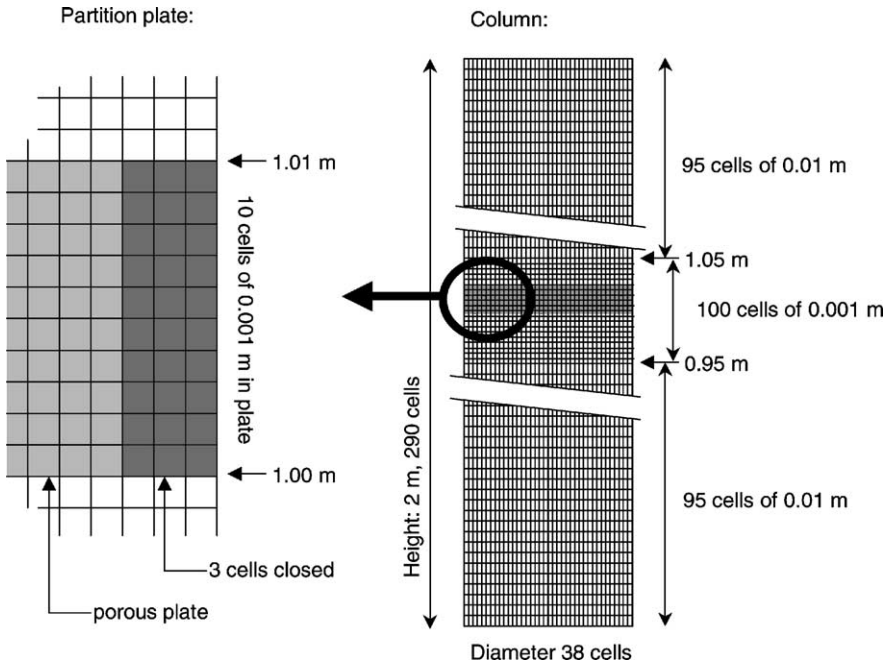


Fig. 4. Grid layout. Complete overview on the right. The inset shows a close up of the side of the column at the height of the partition plate.

At the start of a simulation, water was filled to a height of 1.1 m above the distributor and injection of gas at the bottom was initiated. The small bubbles are injected at the central 32 of 38 cells in radial direction. The large bubbles are injected at the central 22 of 38 cells in radial direction. For all simulations, a time stepping strategy of 20 steps of $5 \times 10^{-4}$ s, 20 steps of $1 \times 10^{-3}$ s, 460 steps of $5 \times 10^{-3}$ s, 500 steps of $1 \times 10^{-2}$ s and 2500 steps of $2 \times 10^{-2}$ s was used. Further details of the simulations as well as animations showing the simulation results can be found at our web site http://ct-cr4.chem.uva.nl/partitionCFD/.

## 3. Simulation results

Fig. 5 shows the transient approach to quasi-steady state for the 0.38 m diameter column operating at

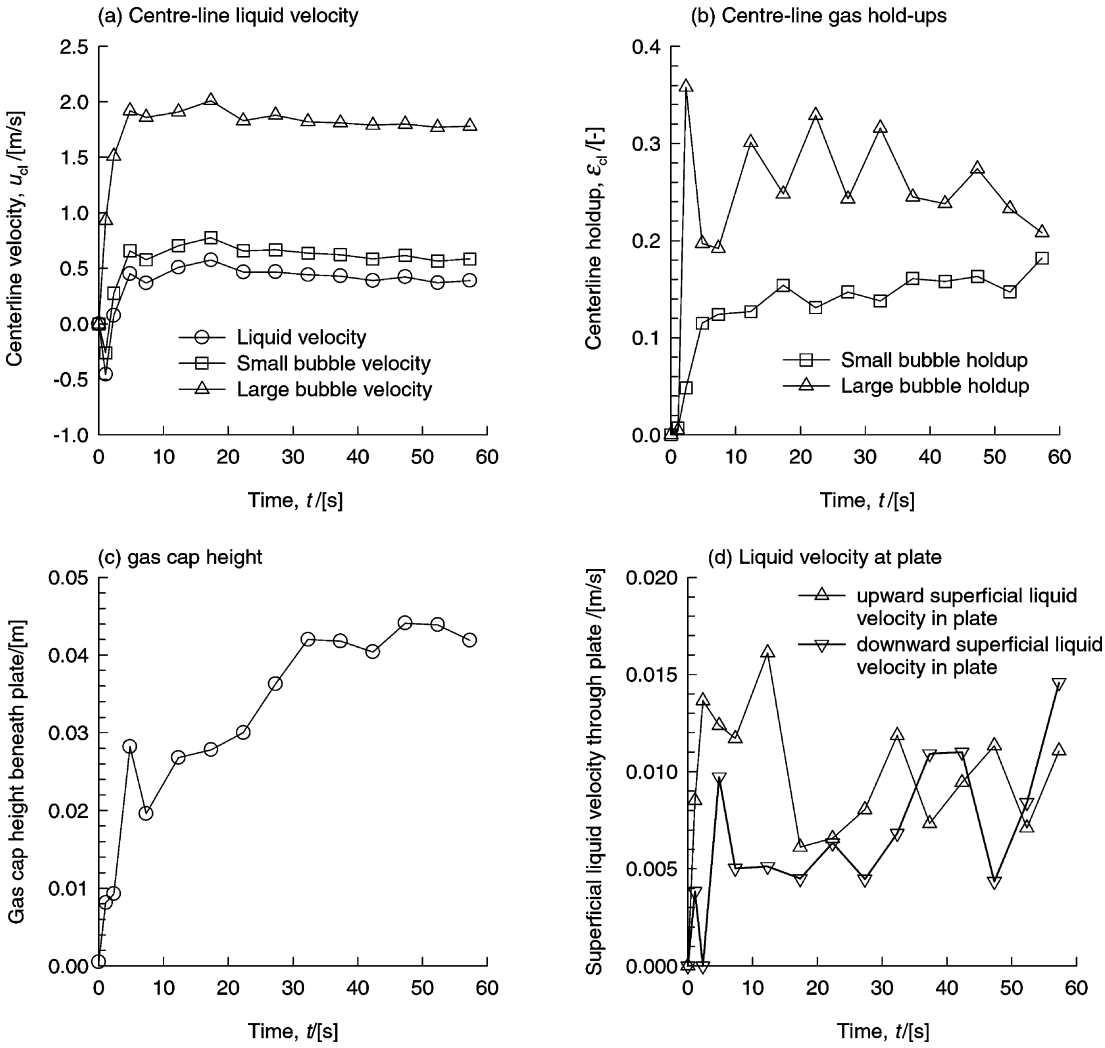


Fig. 5. Transient approach to steady state for a 0.38 m column operating at a superficial gas velocity $U_G = 0.3$ m/s: (a) velocities in the centre of the column at 0.5 m height; these values are representative of the hydrodynamics within the compartment; (b) hold-ups in the centre of the column at 0.5 m height; (c) height of the gas cap that forms below the partition plate; (d) upward- and downward-superficial liquid velocities through the plate. After averaging these will indicate the magnitude of the liquid exchange flow through the partition plate.

$U_G = 0.3$ m/s. Fig. 5(a) shows the liquid velocity at the centre of the column at 0.5 m height for all three phases. Fig. 5(b) shows the hold-up of the small and large bubbles at the same location. Fig. 5(c) shows the height of the gas cap that forms below the plate. The gas cap height below the plate was determined by finding the height at each radial position above which the liquid hold-up dropped below 0.5; this choice is arbitrary. These radial values are averaged to obtain the final value. Fig. 5(d) shows the superficial liquid velocity moving in the upward and downward directions at the plate. The liquid flow up and down through the partition plate were calculated by adding the positive and negative contributions, respectively, of liquid velocity multiplied with liquid hold-up for each cell in radial direction, multiplied with cell-width.

Fig. 6 shows snapshots of the simulations for a superficial gas velocity $U_G = 0.30$ m/s. The vectors indicate liquid velocity. Fig. 6 clearly shows that the

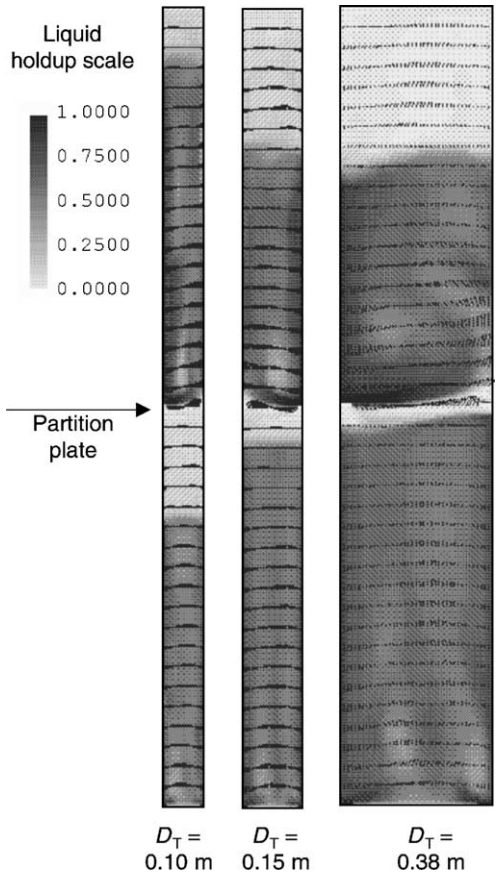


Fig. 6. Snapshots of simulations of 0.10, 0.15 and 0.38 m diameter columns at $U_G = 0.3$ m/s; 18.6% o.a. partition plate. The vectors indicate liquid velocity. The inset on the left indicates the scale used for the liquid hold-up.

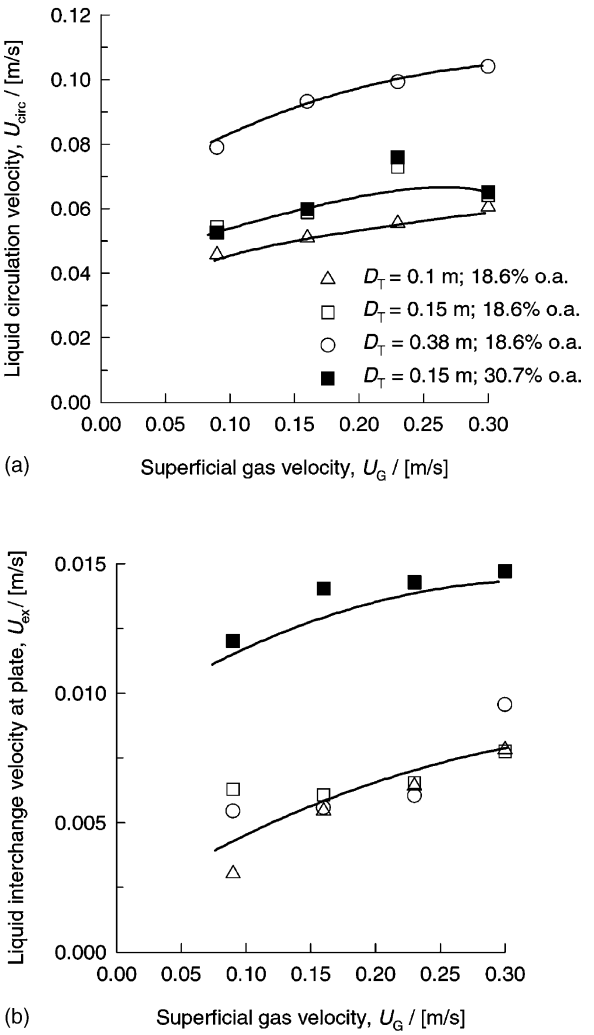


Fig. 7. Simulation results for 0.10, 0.15 and 0.38 m diameter columns for superficial gas velocities of 0.09, 0.16, 0.23 and 0.30 m/s. The open area of the partition plate is either 18.6 or 30.7%: (a) the circulation liquid velocity at 0.5 m height above the distributor. This is representative of the hydrodynamics within each compartment; (b) the superficial velocity of liquid exchange through the partition plate.

gas cap decreases with increasing column diameter, in *qualitative* conformity with the experimental observations (see Fig. 2(c)).

The transient simulation results, such as shown in Fig. 5, were time averaged for the last 20 s to obtain the quasi-steady state values. The steady-state liquid circulation velocities $U_{circ}$ at 0.5 m height above the distributions are shown in Fig. 7(a); these represent the average of the upward- and downward-moving liquid velocities. We note that $U_{circ}$ increases significantly with increasing column diameter; this is in line with the increase of the axial dispersion coefficient $D_{ax}$ in empty bubble columns (see Fig. 2(a)). We also note that $U_{circ}$, within each compartment in the 0.15 m diameter column, is not significantly affected by the open area of the plate. The simulated values of $U_{circ}$ are in *qualitative* agreement with the experimentally determined values reported in Fig. 6 of Dreher and Krishna [3].

The steady-state values of the exchange velocity $U_{ex}$ at the partition plate, obtained by averaging the upward- and downward-velocities (shown in Fig. 5(d)), for the last 20 s of the simulation, are presented in Fig. 7(b). For partition plates of 18.6% o.a., the values of $U_{ex}$ are seen to be independent of the column diameter, in conformity with the experimental results shown in Fig. 2(b). For the 0.15 m diameter column, the values of $U_{ex}$ increase significantly when using partition plates of 30.7% o.a.; these results are again in *qualitative* agreement with those obtained experimentally; see Fig. 2(b).

Comparison of the Fig. 7(a) and (b), shows that the introduction of partition plates reduces the circulation velocities by about one order of magnitude. This result explains the significant reduction in the overall backmixing of the column by introduction of partition plates.

## 4. Conclusions

An important experimental observation in the work of Dreher and Krishna [3] is that the exchange velocity $U_{ex}$ at the partition plate is independent of the column diameter, but depends on the open area of the partition plate; see Fig. 2(b). These experimental findings are confirmed by 2D simulations in the Cartesian framework. There is however no *quantitative* agreement between simulated values of $U_{ex}$ and the experimental values; this is due to 2D simulation strategy adopted. The values of exchange velocity at the partition plate, $U_{ex}$, are about one order of magnitude lower than the circulation velocity within the compartment, $U_{circ}$. This explains the reason behind the efficacy of the partition plate in reducing the overall backmixing in the column.

The simulations also show that the gas cap height formed below the partition plate decreases strongly with increasing column diameter. This is a convenient result from a scale up point of view, because a gas cap represents a waste of reactor volume.

We conclude that 2D Cartesian simulations can be a useful tool in scaling up multi-stage bubble columns.

## Acknowledgements

This research was supported by a grant from the Netherlands Foundation for Scientific Research (NWO) for development of novel concepts in reactive separations technology.

## References

[1] W.D. Deckwer, Bubble Column Reactors, Wiley, New York, 1992.
[2] L.S. Fan, Gas–Liquid–Solid Fluidization Engineering, Butterworths, Boston, 1989.
[3] A.J. Dreher, R. Krishna, Catal. Today 69 (2001) 165–170.
[4] R. Steiner, Chem. Eng. Process. 21 (1987) 1–8.
[5] E. Bartholomé, E. Hetzel, H.C. Horn, M. Molzahn, G.W. Rotermund, L. Vogel, Chem.- Ing.- Tech. 48 (1976) 355–360.
[6] M.B. Kats, L.S. Genin, Int. Chem. Eng. 7 (1967) 246–252.
[7] J. Zahradník, F. Kastánek, Collect. Czech. Chem. Commun. 39 (1974) 1419–1425.
[8] M. Reháková, Z. Novosad, Chem. Eng. Sci. 23 (1968) 139–145.
[9] J. Prenosil, Z. Novosad, Collect. Czech. Chem. Commun. 33 (1968) 3436–3447.
[10] F. Kastánek, J. Zahradník, Collect. Czech. Chem. Commun. 38 (1973) 3725–3741.
[11] F. Zahradník, F. Kastánek, Chem. Eng. Process. 31 (1992) 263–272.
[12] E. Blass, K.H. Koch, Chem.- Ing.- Tech. 44 (1972) 913–921.
[13] E. Blass, W. Cornelius, Chem.- Ing.- Tech. 45 (1973) 236–241.
[14] E. Blass, W. Cornelius, Int. J. Multiphase Flow 3 (1977) 459–469.
[15] T. Sekizawa, H. Kubota, J. Chem. Eng. Jpn. 8 (1975) 507–508.

[16] T. Sekizawa, H. Kubota, J. Chem. Eng. Jpn. 7 (1974) 441–446.
[17] S.N. Palaskar, A.K. De, A.B. Pandit, Chem. Eng. Technol. 23 (2000) 61–69.
[18] A. Kemoun, N. Rados, F. Li, M.H. Al-Dahhan, M.P. Dudukovic, P.L. Mills, T.M. Leib, J.J. Lerou, Chem. Eng. Sci. 56 (2001) 1197–1205.
[19] H.A. Jakobsen, B.H. Sannæs, S. Grevskott, H.F. Svendsen, Ind. Eng. Chem. Res. 36 (1997) 4052–4074.
[20] Y. Pan, M.P. Dudukovic, M. Chang, AIChE J. 46 (2000) 434–449.
[21] J. Sanyal, S. Vasquez, S. Roy, M.P. Dudukovic, Chem. Eng. Sci. 54 (1999) 5071–5083.
[22] A. Sokolichin, G. Eigenberger, Chem. Eng. Sci. 54 (1999) 2273–2284.
[23] R. Krishna, M.I. Urseanu, J.M. van Baten, J. Ellenberger, Chem. Eng. Sci. 54 (1999) 903–4911.
[24] R. Krishna, J.M. van Baten, M.I. Urseanu, Chem. Eng. Sci. 55 (2000) 3275–3286.
[25] R. Krishna, M.I. Urseanu, J.M. van Baten, J. Ellenberger, Chem. Eng. J. 78 (2000) 43–51.
[26] R. Krishna, J.M. van Baten, Chem. Eng. Res. Design, Trans. I. Chem. E. 79 (2001) 283–309.
[27] J.M. van Baten, R. Krishna, Chem. Eng. Sci. 56 (2001) 503–512.
[28] R. Krishna, J.M. van Baten, M.I. Urseanu, J. Ellenberger, Chem. Eng. Sci. 56 (2001) 537–545.
[29] R. Krishna, J.M. van Baten, Chem. Eng. Sci. 56 (2001) 6249–6258.
[30] J.B. Joshi, Chem. Eng. Sci. 56 (2001) 5893–5933.
[31] R. Krishna, J. Ellenberger, AIChE J. 42 (1996) 2627–2634.
[32] L.G. Reilly, D.S. Scott, T.J.W. de Bruijn, D. MacIntyre, Canad. J. Chem. Eng. 72 (1994) 3–12.
[33] T.J. Harmathy, AIChE J. 6 (1960) 281–288.
[34] R. Krishna, M.I. Urseanu, J.M. van Baten, J. Ellenberger, Chem. Eng. Sci. 54 (1999) 171–183.
[35] R. Collins, J. Fluid Mech. 28 (1967) 97–112.
[36] C.M. Rhie, W.L. Chow, AIAA J. 21 (1983) 1525–1532.
[37] J. van Doormal, G.D. Raithby, Numer. Heat Transfer 7 (1984) 147–163.